ADVANCED FUNCTIONAL MATERIALS
www.afm-journal.de

Facile Synthesis of Monodisperse Mesoporous Zirconium Titanium Oxide Microspheres with Varying Compositions and High Surface Areas for Heavy Metal Ion Sequestration

*Dehong Chen, Lu Cao, Tracey L. Hanley, and Rachel A. Caruso**

Monodisperse mesoporous zirconium titanium oxide microspheres with varying compositions (Zr content from 0 to 100%), high surface areas (up to 413 m^2/g) and well-interconnected mesopores are synthesized via a combined sol–gel self-assembly and solvothermal process. Surface areas, pore diameters, crystallinity and mesostructures of the products are controlled by changing the composition of the microspheres. The resulting mesoporous microspheres are tested as adsorbents to remove Cr (VI) anions from solution and the binary oxides show very high adsorption capacities (>25.40 mg/g, that is 0.49 mmol/g) in contrast to previously reported oxides (4.25 mg/g for TiO_2, 4.47 mg/g for α-Fe_2O_3, 5.8 mg/g for CeO_2). The maximum adsorption capacities of the mesoporous microspheres of varying compositions correlate with the amount of surface hydroxyl groups on the materials. A maximum adsorption capacity of 29.46 mg/g (0.57 mmol/g) is achieved on the microspheres containing 30% Zr due to abundant active hydroxyl groups for heavy metal ion adsorption. Owing to their integrated features (including variable compositions, high specific surface area, tunable pore size and monodisperse grain size) as well as specific acid-base surface properties, such mesoporous zirconium titanium oxide microspheres are also expected to have potential either as catalysts or catalyst supports for industrial applications.

1. Introduction

Due to their specific functional characteristics and importance in a wide variety of technical fields, titania, zirconia and their binary oxides have been widely employed in fields including photocatalysis, dye-sensitized solar cells, catalysis, photoluminescence, capillary electrophoresis, chromatography, inorganic pigments, dielectric ceramics, heavy metal ion and radioactive waste (radwaste) sequestration.[1–10] Recently the exploitation of these oxides for heavy metal ion and radwaste sequestration has attracted attention because of their demonstrated superior thermal, chemical, hydrolytic and radiolytic stabilities, as well as outstanding durability for long term service.[11–17] In contrast to the individual titania or zirconia, the zirconium titanium binary oxide shows enhanced thermal stability as the presence of -Zr-O-Ti-O-Zr- networks can retard the nucleation and crystallization of the individual parent components, therefore giving rise to an amorphous binary metal oxide matrix with high specific surface area and adjustable porosity.[14,15] These controllable characteristics of the binary metal oxide would be beneficial for metal ion adsorption owing to the increase in the amount and density of the adsorption sites. Moreover, such zirconium titanium oxides also exhibit modifiable surface properties, which could promote the applicability of the resulting oxide as a high performance adsorbent.[3,17,18]

In large scale solid liquid column separation processes the morphology of solid materials is a vital factor. Spherical particles with monodisperse size and robust frameworks are preferred due to their unique packing ability, which can give rise to efficient separation processes.[17–20] Although considerable efforts have been devoted to the preparation of diverse binary zirconium titanium oxide materials,[16,17,21–24] to the best of our knowledge, a general method for the synthesis of zirconium titanium binary oxide microspheres in which the composition can be varied simply, giving monodisperse particle size and the ability to finely-adjust porosity is rarely reported.[18,19]

Herein, a facile sol–gel self-assembly and solvothermal process has been demonstrated to prepare monodisperse mesoporous zirconium titanium oxide microspheres. The compositions of the binary oxides were varied from 0 to 100% Zr resulting in high surface areas up to 413 m^2/g. The spherical particles contained well-interconnected mesopores throughout. The crystallinity and mesostructure of the final zirconium titanium oxide microspheres are tunable by the subsequent solvothermal treatment, thereby allowing control of the specific surface areas and pore diameters of the materials. Amorphous

Dr. D. H. Chen, L. Cao, Prof. R. A. Caruso
PFPC, School of Chemistry
The University of Melbourne
Melbourne, Victoria 3010, Australia
E-mail: rcaruso@unimelb.edu.au
Dr. T. L. Hanley
Institute of Materials Engineering
ANSTO, Locked Bag 2001, Kirrawee DC, NSW 2232, Australia
Prof. R. A. Caruso
CSIRO Materials Science and Engineering
Private Bag 33, Clayton South, Victoria 3169, Australia

DOI: 10.1002/adfm.201102878

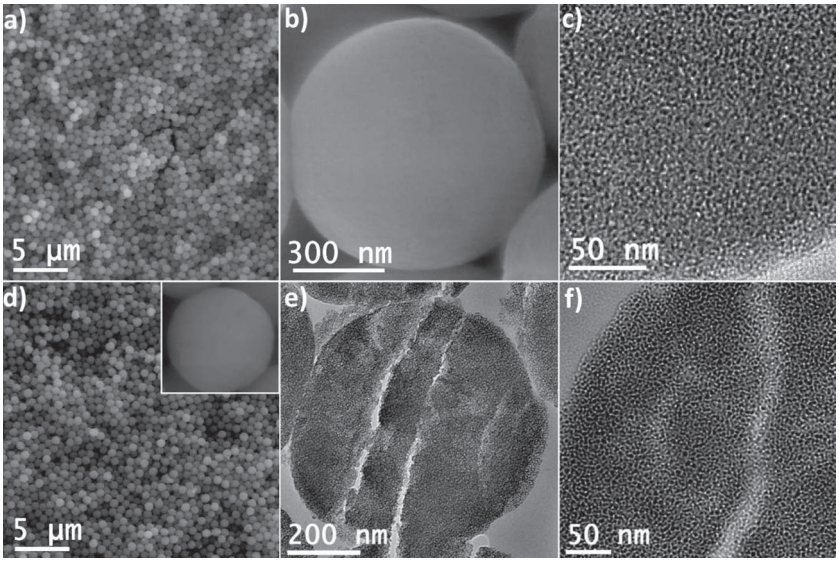

Figure 1. SEM images of the 50Zr50Ti oxide microspheres and the corresponding TEM images of the ultramicrotomed sample: a), b) and c) as-prepared precursor microspheres, d), e) and f) solvothermally-treated and then calcined microspheres. Inset in d) is a higher magnification SEM image of a single calcined microsphere (image size 860 nm × 800 nm). Note: all the SEM images were obtained without sputter coating. The parallel ridgelines observed for the sample in e) and f) were a result of the ultramicrotoming process during TEM sample preparation.

binary oxide microspheres with high surface areas (>280 m^2/g) and uniform mesopores (~5.5 nm) can be prepared when the Zr content ranges from 30 to 80%. In contrast, the Zr- or Ti-rich precursor microspheres (>90% Zr or <20% Zr) tend to crystallize into zirconia or anatase nanocrystals, respectively, during either the solvothermal treatment or calcination process. The resultant zirconium titanium oxide microspheres have been employed as adsorbents for sorption of the heavy metal ion Cr (VI) from solution. The binary oxides show very high adsorption capacities in contrast to previously investigated oxides (4.25 mg/g for TiO_2, 4.47 mg/g for α-Fe_2O_3, 5.8 mg/g for CeO_2)[25,26] with a maximum adsorption capacity of 29.46 mg/g (0.57 mmol/g) achieved on the mesoporous 30Zr70Ti (30 mol.% Zr–70 mol.% Ti) oxide microspheres, indicating their potential for application in the water purification field. This facile and reproducible approach is an important step toward the synthesis of mesoporous oxide microspheres for environmental cleanup and industrial catalysis applications.

2. Results and Discussion

For all sample compositions studied the sol–gel self-assembly in the presence of hexadecylamine (HDA) resulted in monodisperse spheres with diameters less than a micrometer (see **Figure 1**a). The electron microscopy images in Figure 1a–c show the precursor spheres obtained using a 1:1 molar ratio of Zr to Ti during synthesis. For all samples the precursor spheres had relatively smooth surfaces (as an example, Figure 1b), without granular features, indicating ultrafine primary particles less than 10 nm within the sphere structure. The mesostructure observed from TEM analysis of the ultramicrotomed samples was worm-hole like (Figure 1c); this was confirmed with the corresponding SAXS pattern (Supporting Information, Figure S1). After solvothermal treatment of these precursor spheres at 433 K and then calcination at 773 K the monodispersity (Figure 1d) and smooth surface of the spheres were retained (Figure 1d inset). The diameter of the spheres (780 ± 40 nm) was not altered significantly during the heating processes. The original worm-hole like mesostructure in the precursor spheres is retained in the calcined sample as worm-hole like mesopores throughout the microsphere (Figure 1e and f).

SAXS patterns of the samples after solvothermal treatment and calcination at 773 K show a broad reflection for the calcined samples prepared using less than 80% Ti content (**Figure 2**a), indicating the presence of worm-hole like pore structuring. This reflection is no longer apparent with samples prepared using ≥80% Ti content as anatase crystals (>40 nm) are formed in the sample, as discussed below, disrupting the mesostructure.

The corresponding wide angle XRD patterns are shown in Figure 2b. Anatase crystals were present in the samples prepared using ≥ 80% Ti content as there was insufficient ZrO_2 present to prevent crystal growth. As the amount of zirconia in the sample increased, the samples were amorphous even after calcination at 773 K. This would indicate that the Ti and Zr species were well distributed within the microspheres, preventing sufficient size domains of either species to occur and therefore crystallize during calcination.[14,22] Taking the 50Zr50Ti oxide microspheres as an example, no crystal phases of either titania

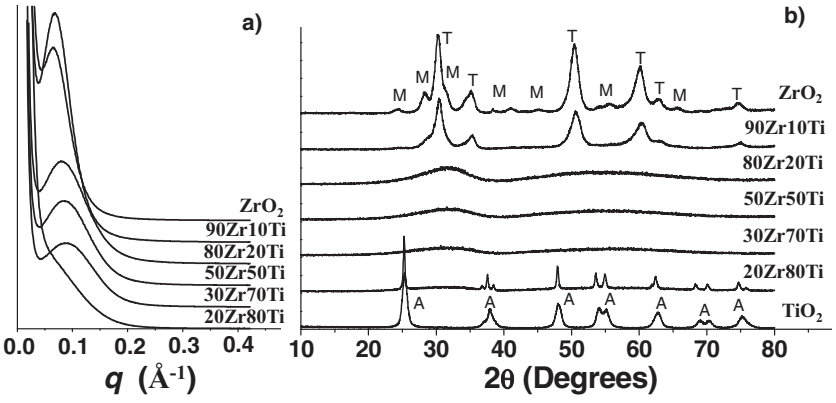

Figure 2. a) SAXS and b) wide angle XRD patterns of the solvothermally-treated and calcined zirconium titanium oxide microspheres prepared with varying Zr/Ti molar ratios. A = anatase titania, M = monoclinic zirconia and T = tetragonal zirconia.

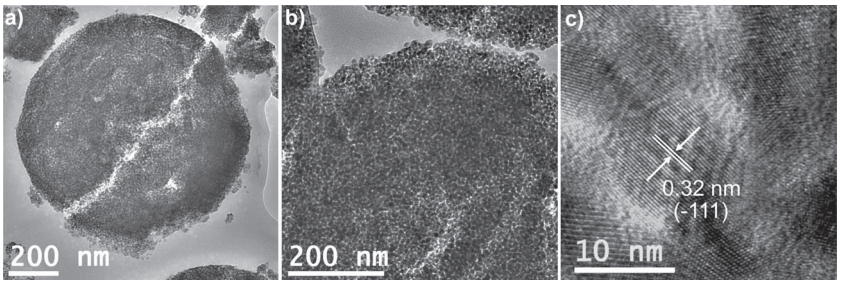

Figure 3. TEM images a) and b) of the ultramicrotomed zirconia microsphere solvothermally treated and then calcined at 773 K, and c) HRTEM image of the zirconia nanocrystals in the framework of the mesoporous microsphere. The parallel ridgelines observed for the sample in a) and b) were a result of the ultramicrotoming process during TEM sample preparation.

or zirconia nanocrystals were found after calcination at temperatures up to 873 K (see Supporting Information, Figure S2), suggesting a relatively high thermal stability of the resulting amorphous microsphere.[14] Increasing the calcination temperature to 973 K resulted in a direct crystallization into orthorhombic $ZrTiO_4$ (see Supporting Information, Figure S2 and S3). The samples prepared using 90% Zr contained tetragonal phase zirconia nanocrystals as the presence of Ti^{4+} is known to prevent the formation of monoclinic zirconia,[14] and the pure zirconia sample consisted of both tetragonal and monoclinic zirconia nanocrystals. These crystals were small (<10 nm) as determined by the peak broadening in the wide angle XRD patterns (Figure 2b) and as observed in the TEM images (**Figure 3**). Interestingly, even with the growth of these crystals, the worm-hole like mesopores are still observed in the final microspheres as indicated by SAXS patterns (Figure 2a) and TEM images (Figure 3). The TEM images (Figure 3a and b) of the pure zirconia microspheres after solvothermal treatment and calcination show a granular nature due to the presence of the zirconia nanocrystals. High resolution TEM images (for example, Figure 3c) and calculations from the wide angle XRD patterns confirm the nanocrystals are <10 nm in diameter. Such a small crystal size is essential to prevent disruption to the mesostructure.[28,29] As shown in the HRTEM image (Figure 3c), the lattice fringes with a spacing of 0.32 nm can be correlated to the (-111) planes of the monoclinic zirconia (JCPDS 72-1669), indicating a well-crystallized inorganic framework in the final product.

From gas sorption studies, **Figure 4**, type IV isotherms with obvious hysteresis loops were observed for all the calcined microspheres indicating the presence of mesopores.[30] This result is in good agreement with those derived from both SAXS and TEM characterizations. For the calcined 30Zr70Ti oxide microspheres, a very high specific surface area of 413 m^2/g was attained due to the small subunit particles (~3.5 nm determined by TEM, Supporting Information Figure S4). The shift of the hysteresis loop to lower relative pressure with increasing Zr content in the mixed composition materials suggests a decrease in the pore size. From the pore size distribution curves shown in Figure 4b, the peak in pore size can be seen to decrease substantially from the pure TiO_2 sample to the samples prepared with 20, 50 and 80% Zr, and increase again for the pure ZrO_2 sample. The presence of crystals within the pure TiO_2 and ZrO_2 samples obviously vary the mesostructure relative to the amorphous samples. In addition, the variation in the shape of the hysteresis loops observed in the isotherms suggests that the pore shape alters with composition. As shown in **Table 1**, the calcined Zr–Ti mixed oxide samples possess high specific surface areas, revealing the interconnected nature of the worm-hole like mesopores. This result is in agreement with that from the TEM observation.

Due to the high specific surface area and abundance of well-interconnected mesopores, the resulting zirconium titanium oxide microspheres were expected to show promise in the uptake of heavy metal ions for water purification applications. Chromium was chosen as a probe to illustrate the adsorption capability of the resulting zirconium titanium oxide microspheres. **Figure 5** shows the typical adsorption isotherms of the zirconium titanium oxide microspheres with varying compositions. The adsorption data were fitted using the Langmuir model and the corresponding maximum adsorption capacity, Q_{max} (mg/g), relating to complete monolayer coverage and correlation coefficient are given in **Table 2**. The highest adsorption capacity of 29.46 mg/g (0.57 mmol/g) was achieved on the 30Zr70Ti oxide microspheres due to its very high specific surface area of 413 m^2/g. The mesoporous binary oxide microspheres with relatively high Zr contents (40Zr, 60Zr and 80Zr)

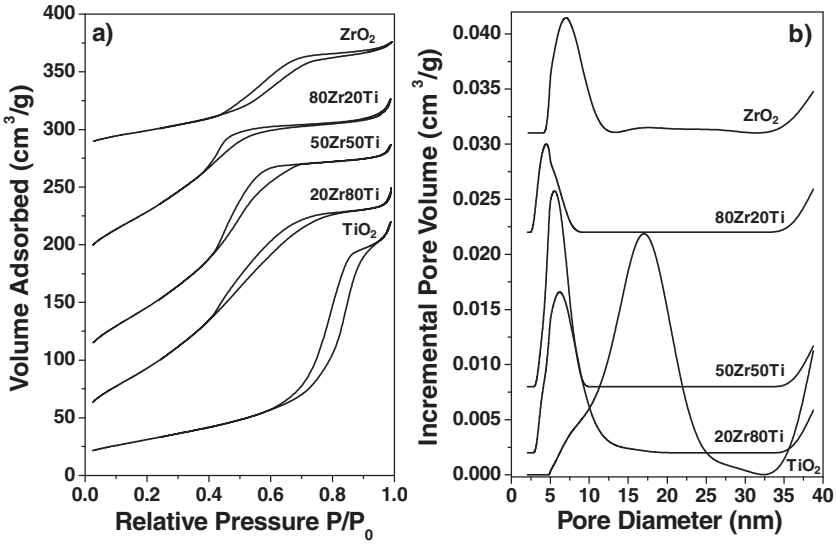

Figure 4. a) Nitrogen sorption isotherms of the calcined zirconium titanium oxide microspheres synthesized with varying Zr/Ti molar ratio and b) the corresponding pore size distribution determined by using the NLDFT method based on the oxide cylindrical pore model for N_2 at 77 K. The 20Zr80Ti, 50Zr50Ti, 80Zr20Ti and ZrO_2 curves are shifted in vertical axis by 10, 60, 150 and 270 cm^3/g in a) and 0.002, 0.008, 0.022 and 0.031 cm^3/g in b) for clarity.

Table 1. Physical properties of the calcined mesoporous zirconium titanium oxide microspheres.[a)]

Sample name	S_{BET} [m^2/g]	PSD [nm]	V_{sp} [cm^3/g]	Crystal phase
TiO_2	108	17	0.313	Anatase TiO_2
10Zr90Ti oxide	73	23	0.406	Anatase TiO_2 & Amorphous
20Zr80Ti oxide	304	6.2	0.356	Anatase TiO_2 & Amorphous
30Zr70Ti oxide	413	4.9	0.389	Amorphous
40Zr60Ti oxide	367	5.5	0.397	Amorphous
50Zr50Ti oxide	315	5.6	0.345	Amorphous
60Zr40Ti oxide	321	5.5	0.348	Amorphous
70Zr30Ti oxide	306	5.6	0.327	Amorphous
80Zr20Ti oxide	283	4.5	0.266	Amorphous
90Zr10Ti oxide	212	4.8	0.201	Tetragonal ZrO_2
ZrO_2	104	7.0	0.161	Monoclinic & Tetragonal ZrO_2

[a)] S_{BET} = BET specific surface area obtained from N_2 adsorption data in the P/P_0 range from 0.05 to 0.20. PSD = pore size distribution determined by using the NLDFT method based on the oxide cylindrical pore model for N_2 at 77 K. V_{sp} = single-point pore volume calculated from the adsorption isotherm at $P/P_0 = 0.98$.

Table 2. Cr (VI) uptake capacity of the calcined mesoporous zirconium titanium oxide microspheres of varying compositions.[a)]

Sample name	Q_{max} [mg/g]	R^2	Site density [#Cr/nm^2]	OH amount [mmol/g]	OH density [#/nm^2]	#OH/#Cr (VI) mole ratio
TiO_2	9.93	0.92	1.0	0.74	4.1	3.9
30Zr70Ti oxide	29.46	0.96	0.8	2.06	3.0	3.6
40Zr60Ti oxide	26.87	0.96	0.8	1.77	2.9	3.4
60Zr40Ti oxide	25.54	0.98	0.9	1.75	3.3	3.6
80Zr20Ti oxide	25.40	0.97	1.0	1.79	3.6	3.7
ZrO_2	17.17	0.94	1.9	1.07	6.2	3.2

[a)] Q_{max} = maximum adsorption capacity obtained by fitting with Langmuir model and refers to the total amount of Cr (VI) atom derived from $HCrO_4^-$, CrO_4^{2-} and $Cr_2O_7^{2-}$ species. R^2 = correlation coefficient. Site density = $(Q_{max} \times 10^{-3} \times 6.02 \times 10^{23})/(52 \times S_{BET} \times 10^{18})$. OH densities of the resulting oxide microspheres were determined using a TGA method according to Ref-35. #OH/#Cr (VI) = mole ratio of the surface hydroxyl groups to the adsorbed Cr (VI) derived from $HCrO_4^-$, CrO_4^{2-} and $Cr_2O_7^{2-}$ species.

also had very high Cr adsorption capability (>25.40 mg/g) compared with the previously investigated oxides (4.25 mg/g for TiO_2, 4.47 mg/g for α-Fe_2O_3, 5.8 mg/g for CeO_2).[25,26] As shown in **Figure 6**a, the maximum adsorption capacity (Q_{max}) of the resulting mesoporous microspheres did not directly correlate with the specific surface areas of the materials.

As the metal uptake experiments were conducted at pH = 3, the Cr (VI) exists as anionic species in the solution: $HCrO_4^-$, CrO_4^{2-} or $Cr_2O_7^{2-}$.[31] This pH is below the point of zero charge (PZC) of either titania or zirconia (PZC_{TiO2}: pH = 5.9 and PZC_{ZrO2}: pH = 6.5),[32,33] hence the surfaces of the oxides were positively charged due to the presence of abundant protonated hydroxyl groups.[34] Thus the adsorption of the Cr (VI) anions to the surfaces is believed to occur via electrostatic interactions,[30,34] making the hydroxyl group density of the resulting zirconium titanium oxide microspheres an important parameter for consideration. The hydroxyl group density was determined using a thermogravimetric analysis method,[35] and the results are shown in Table 2. The pure titania or zirconia samples had higher hydroxyl densities than the other zirconium titanium oxide microspheres, and the 40Zr60Ti oxide microspheres were found to possess a minimum hydroxyl density of 2.9 OH/nm^2. This observed trend is quite similar to that reported for similar composition materials.[15] As shown in Figure 6b, the maximum adsorption capacities of the mesoporous microspheres do vary with the hydroxyl group quantity on the samples. This result suggests that mesopores inside the microsphere are well-interconnected, therefore resulting in the surface hydroxyl groups being readily accessible for the Cr (VI) anions.

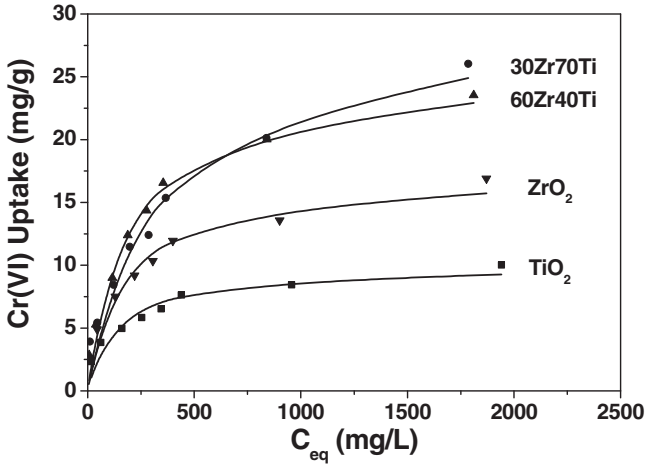

Figure 5. Typical adsorption isotherms of the mesoporous zirconium titanium oxide microspheres with varying compositions. The solid lines are fitted results using the Langmuir model.

3. Conclusions

Mesoporous zirconium titanium oxide microspheres with varying compositions (Zr content from 0 to 100%), high specific surface areas (up to 413 m^2/g), uniform worm-hole like mesopores (~5.5 nm) and monodisperse grain size (780 ± 40 nm) can be fabricated using a facile sol–gel and solvothermal process. Crystallinity and mesostructures of the resulting microspheres are tunable by adjusting their compositions: mesoporous microspheres containing well-crystallized zirconia nanocrystals, an amorphous binary oxide matrix or anatase titania nanocrystals can be prepared when the Zr content was higher than 90%, between 30% and 80%, or less than 20%, respectively. The mesoporous binary oxide microspheres have very high adsorption capability (>25.40 mg/g, that is 0.49 mmol/g) for Cr (VI) anions in aqueous solution, showing a high potential for heavy metal ion sequestration applications.

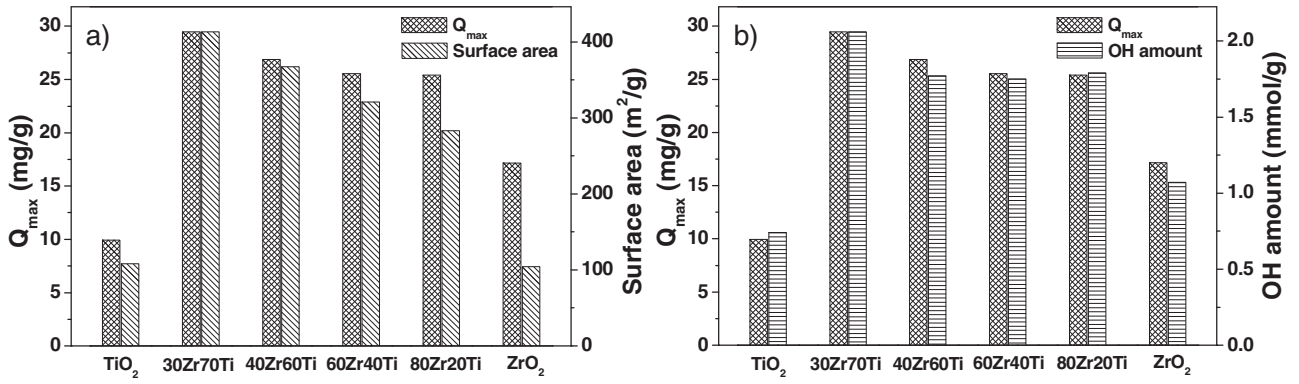

Figure 6. Relationships between maximum adsorption capacities (Q_{max}) and a) specific surface areas and b) hydroxyl amounts of the resulting mesoporous zirconium titanium oxide microspheres.

4. Experimental Section

Chemicals: Titanium(IV) isopropoxide (TIP, 97%), zirconium(IV) propoxide (ZrP, 70 wt.% in 1-propanol), 1,5-diphenylcarbazide (ACS reagent) and hexadecylamine (HDA, 90%) were purchased from Sigma-Aldrich and used as received. Absolute ethanol (>99.5% Chem-Supply), acetone (>99.5% Chem-Supply), potassium chloride (AR, BDH), and hydrochloric acid (37%, Scharlau) were used as received. Potassium dichromate (AJAX chemicals, >99.7%) was dried at 393 K for 2 h before preparing solutions. Milli-Q water (18.2 MΩ cm) was used for solution preparation and synthesis.

Synthesis: The nonporous precursor microspheres were prepared via a sol–gel self-assembly process in the presence of HDA as a structure-directing agent. The HDA was used to alter the hydrophilicity of the hydrolyzed titanium and zirconium species/oligomers and initiate the self-assembly process.[36,37] The solution composition of ZrP: TIP: HDA: H_2O: KCl: ethanol (molar ratio) was varied in the range of ($0 \leq x \leq 1$): (1-x): 1: 3: 5.5×10^{-3}: 236.5. In a typical synthesis of the 50Zr50Ti (Zr:Ti = 1:1 in molar ratio) binary oxide microspheres, 15.90 g HDA was dissolved in 790 mL ethanol, followed by the addition of 3.20 mL KCl solution (0.1 M). To this solution, a well-mixed alkoxide solution of 10 mL ethanol, 14.04 g ZrP and 8.79 g TIP was added under vigorous stirring at ambient temperature. The resulting milky white precursor bead suspension was kept static at room temperature for 18 h, then the precursor microspheres were collected by centrifugation, washed with ethanol three times and dried in air at ambient temperature. In order to prepare mesoporous zirconium titanium oxide microspheres, the precursor microspheres underwent a solvothermal treatment. 1.6 g of the precursor microspheres were dispersed in a 20 mL ethanol and 10 mL Milli-Q water mixture. The resulting mixtures were sealed within a Teflon-lined autoclave (50 mL) and heated at 433 K for 16 h. The solid products were then collected by filtration, washed with ethanol three times, and dried in air at room temperature. Finally, the air-dried powders were calcined at 773 K for 2 h in air to remove organic components and produce the mesoporous zirconium titanium oxide microspheres for characterization. Such calcined materials were denoted as xZr(100-x)Ti oxide microspheres, where x = Zr·100/(Zr + Ti) in mole ratio. It is worth noting that solvothermal treatment prior to calcination is a necessary step to attain high specific surface areas and uniform mesopores of the resultant oxide microspheres.[36,38] When the nonporous precursor microspheres were directly calcined in air, the resulting oxide microspheres possess much lower specific surface areas, smaller pore diameters and pore volumes relative to the solvothermally-treated and calcined counterparts heated at the same temperature (See table S1 in the supporting information).

Cr (VI) Adsorption Experiment: The pH value of the potassium chromate solution was adjusted to 3 with hydrochloric acid (0.1 M) prior to the adsorption experiments to ensure species of Cr (VI) as negative charged anions. Cr (VI) adsorption isotherms on the mesoporous microspheres were obtained using batch contact methodology in which the powdered adsorbent was contacted with solutions containing the target species in a volume/mass ratio of 100 mL/g. That is 200 mg of the mesoporous microspheres were suspended in 20 mL Cr (VI) solution in a 28 mL screw-capped container with initial concentrations ranging from 50 to 2000 mg/L (0.96 to 38.46 mmol/L). The containers were wrapped with aluminium foil and shaken at 298 K for 48 h. Then the mesoporous microspheres were removed using a syringe filter with a 0.2 μm hydrophilic polyethersulfone membrane (Pall corporation, USA) and the concentration of the Cr (VI) in the filtrate was analyzed on a UV–vis spectrophotometer (Cary 50 Bio) using 1,5-diphenylcarbazide as the color agent at the wavelength of 544 nm.[27] Pre-dried potassium dichromate was used to prepare standard Cr (VI) solutions with concentrations ranging from 0.5 to 5 mg/L and colored with 1,5-diphenylcarbazide. The corresponding absorbance values corrected with blank solvent were recorded on the UV-Vis spectrophotometer. A calibration curve was obtained by plotting the resulting absorbance values against standard concentrations (mg/L) of the Cr (VI) solution and it was used to determine the Cr (VI) concentrations of the filtrate with appropriate dilution.

The adsorption data were fitted with the Langmuir model described as follows:[16,19]

$$C_{ads} = \frac{Q_{max} b C_{eq}}{1 + b C_{eq}}$$

where C_{ads} (mg/g) and C_{eq} (mg/L) are the equilibrium concentration in the solid and liquid phases, respectively. Q_{max} (mg/g) is the maximum adsorption capacity associated with complete monolayer coverage and b is a Langmuir constant related to the energy and affinity of the sorbent.

Characterization: The morphologies of the samples were observed by using a field emission Environmental Scanning Electron Microscope (Quanta 200F FEI) under low vacuum mode. In order to observe genuine fine structures on the external surface, the samples were observed without metal sputter coating. For transmission electron microscopy (TEM) and selected area electron diffraction (SAED) characterization, the samples were embedded in an LR-white resin and ultramicrotomed to 60 nm-thick sections, then loaded onto Cu grids coated with holey carbon films and observed on a FEI Tecnai F20 transmission electron microscope operating at 200 kV. The crystalline phase of the product was determined using powder X-ray diffraction (XRD, Bruker D8 Diffractometer with Cu Kα radiation). The samples were scanned from 5 to 80 degrees at a step size of 0.02 degrees and a scan step time of 4 sec. Small angle X-ray scattering (SAXS) patterns of the samples were recorded on a laboratory based 3-pinhole SAXS system (Bruker Nanostar). The instrument source was a copper rotating anode (0.3 mm filament) operating at 45 kV and 110 mA, fitted with cross-coupled Montel mirrors, resulting in Cu Kα radiation of wavelength 1.54 Å. The

SAXS camera was fitted with a Vantec 2000 2D detector (effective pixel size 60 μm). The optics and sample chamber were under vacuum to minimize air scatter. The sample to detector distance was chosen to be 710 mm, which provided a q-range of 0.01 to 0.42 $Å^{-1}$. The pH values of the Cr (VI) aqueous solution were measured using an OAKTON pH/mV 11 meter. Prior to the measurement, the electrode was calibrated using fresh standard pH buffer solutions. Thermogravimetric and differential thermal analysis (TGA-DTA) measurements were made on a Mettler Toledo TGA/SDTA851^e module at a heating rate of 10 K/min under flowing air. Nitrogen sorption isotherms were measured at 77 K by using a Micromeritics Tristar 3000 surface area and porosity analyzer. The calcined samples were degassed at 433 K on a vacuum line for 18 h prior to the measurement. The adsorption data in the P/P_0 range from 0.05 to 0.20 were utilized to calculate the specific surface area using a standard multi-point Brunauer–Emmett–Teller (BET) method. A non-localized density functional theory (NLDFT) method was used to determine the pore size distribution based on an oxide cylindrical pore model for N_2 at 77 K.

Supporting Information

Supporting Information is available from the Wiley Online Library or from the author.

Acknowledgements

This research was financially supported by an Australian Research Council Discovery Project (DP0877428) and AINSE Award (AINGRA10120). RAC is a recipient of an Australian Research Council Future Fellowship (FT0990583). Dr Simon Crawford is thanked for ultramicrotoming samples in preparation for TEM characterization. The Electron Microscopy Unit of the Bio21 Institute at The University of Melbourne is acknowledged for electron microscopy access.

Received: November 28, 2011
Published online: February 16, 2012

[1] X. Chen, S. S. Mao, *Chem. Rev.* **2007**, *107*, 2891.
[2] J. Rappsilber, M. Mann, Y. Ishihama, *Nat. Protoc.* **2007**, *2*, 1896.
[3] B. M. Reddy, A. Khan, *Catal. Rev.-Sci. Eng.* **2005**, *47*, 257.
[4] M. Grätzel, *Nature* **2001**, *414*, 338.
[5] D. H. Chen, F. Z. Huang, Y. B. Cheng, R. A. Caruso, *Adv. Mater.* **2009**, *21*, 2206.
[6] L. Li, C. K. Tsung, Z. Yang, G. D. Stucky, L. D. Sun, J. F. Wang, C. H. Yan, *Adv. Mater.* **2008**, *20*, 903.
[7] F. Sauvage, D. H. Chen, P. Comte, F. Z. Huang, L. P. Heiniger, Y. B. Cheng, R. A. Caruso, M. Graetzel, *ACS Nano* **2010**, *4*, 4420.
[8] F. Z. Huang, D. H. Chen, X. L. Zhang, R. A. Caruso, Y. B. Cheng, *Adv. Funct. Mater.* **2010**, *20*, 1301.
[9] D. J. Yang, Z. F. Zheng, H. Y. Zhu, H. W. Liu, X. P. Gao, *Adv. Mater.* **2008**, *20*, 2777.
[10] M. Dondi, F. Matteucci, G. Cruciani, *J. Solid State Chem.* **2006**, *179*, 233.
[11] G. I. Spijksma, C. Huiskes, N. E. Benes, H. Kruidhof, D. H. A. Blank, V. G. Kessler, H. J. M. Bouwmeester, *Adv. Mater.* **2006**, *18*, 2165.
[12] B. Savoini, D. Caceres, I. Vergara, R. Gonzalez, J. E. M. Santiuste, *J. Nucl. Mater.* **2000**, *277*, 199.
[13] K. Kuramoto, H. Mitamura, T. Banba, S. Muraoka, *Prog. Nucl. Energy* **1998**, *32*, 509.
[14] M. E. Manriquez, M. Picquart, X. Bokhimi, T. Lopez, P. Quintana, J. M. Coronado, *J. Nanosci. Nanotechnol.* **2008**, *8*, 6623.
[15] H. Zou, Y. S. Lin, *Appl. Catal. A* **2004**, *265*, 35.
[16] G. L. Drisko, V. Luca, E. Sizgek, N. Scales, R. A. Caruso, *Langmuir* **2009**, *25*, 5286.
[17] C. S. Griffith, G. D. Sizgek, E. Sizgek, N. Scales, P. J. Yee, V. Luca, *Langmuir* **2008**, *24*, 12312.
[18] G. D. Sizgek, C. S. Griffith, E. Sizgek, V. Luca, *Langmuir* **2009**, *25*, 11874.
[19] G. D. Sizgek, E. Sizgek, C. S. Griffith, V. Luca, *Langmuir* **2008**, *24*, 12323.
[20] J. H. Pan, X. W. Zhang, A. J. Du, D. D. Sun, J. O. Leckie, *J. Am. Chem. Soc.* **2008**, *130*, 11256.
[21] R. F. de Farias, C. Airoldi, *J. Colloid Interface Sci.* **1999**, *220*, 255.
[22] V. Luca, W. K. Bertram, J. Widjaja, D. R. G. Mitchell, C. S. Griffith, E. Drabarek, *Microporous Mesoporous Mater.* **2007**, *103*, 123.
[23] S. V. Pol, V. G. Pol, A. Gedanken, G. I. Spijksma, J. Grinblat, R. K. Selvan, V. G. Kessler, G. A. Seisenbaeva, S. Gohil, *J. Phys. Chem. C* **2007**, *111*, 2484.
[24] Q. Yuan, Y. Liu, L. L. Li, Z. X. Li, C. J. Fang, W. T. Duan, X. G. Li, C. H. Yan, *Microporous Mesoporous Mater.* **2009**, *124*, 169.
[25] J. S. Hu, L. S. Zhong, W. G. Song, L. J. Wan, *Adv. Mater.* **2008**, *20*, 2977.
[26] F. Jiang, Z. Zheng, Z. Y. Xu, S. R. Zheng, Z. B. Guo, L. Q. Chen, *J. Hazard. Mater.* **2006**, *134*, 94.
[27] US EnvironmentalProtection Agency (EPA) method 7196A, Chromium Hexavalent (Colorimetric), http://www.epa.gov/osw/hazard/testmethods/sw846/pdfs/7196a.pdf.
[28] J. Ba, J. Polleux, M. Antonietti, M. Niederberger, *Adv. Mater.* **2005**, *17*, 2509.
[29] Q. Yuan, Q. Liu, W. G. Song, W. Feng, W. L. Pu, L. D. Sun, Y. W. Zhang, C. H. Yan, *J. Am. Chem. Soc.* **2007**, *129*, 6698.
[30] S. Lowell, J. E. Shields, M. A. Thomas, M. Thommes, *Characterization of Porous Solids and Powders: Surface Area, Pore Size and Density*, Kluwer, London **2004**.
[31] Y. Ku, I.-L. Jung, *Water Res.* **2001**, *35*, 135.
[32] M. Kosmulski, *Adv. Colloid Interface Sci.* **2002**, *99*, 255.
[33] M. Kosmulski, *J. Dispersion Sci. Technol.* **2002**, *23*, 529.
[34] W. Stumm, *Chemistry of the Solid-Water Interface: Processes at the Mineral-Water and Particle-Water Interface in Natural Systems*, John Wiley & Sons, Inc., New York **1992**.
[35] R. Mueller, H. K. Kammler, K. Wegner, S. E. Pratsinis, *Langmuir* **2002**, *19*, 160.
[36] D. H. Chen, L. Cao, F. Z. Huang, P. Imperia, Y. B. Cheng, R. A. Caruso, *J. Am. Chem. Soc.* **2010**, *132*, 4438.
[37] G. A. Soler-Illia, C. Sanchez, B. Lebeau, J. l. Patarin, *Chem. Rev.* **2002**, *102*, 4093.
[38] D. H. Chen, Z. Li, C. Z. Yu, Y. F. Shi, Z. D. Zhang, B. Tu, D. Y. Zhao, *Chem. Mater.* **2005**, *17*, 3228.